Do bacterial L-asparaginases utilize a catalytic triad Thr-Tyr-Glu?[1]

Khosrow Aghaiypour [2], Alexander Wlodawer, Jacek Lubkowski *

Macromolecular Crystallography Laboratory, National Cancer Institute at Frederick, Frederick, MD 21702, USA

Abstract

The structures of *Erwinia chrysanthemi* L-asparaginase (ErA) complexed with the L- and D-stereoisomers of the suicide inhibitor, 6-diazo-5-oxy-norleucine, have been solved using X-ray crystallography and refined with data extending to 1.7 Å. The distances between the Cα atoms of the inhibitor molecules and the hydroxyl oxygen atoms of Thr-15 and Tyr-29 (1.20 and 1.60 Å, respectively) clearly indicate the presence of covalent bonds between these moieties, confirming the nucleophilic role of Thr-15 during the first stage of enzymatic reactions and also indicating direct involvement of Tyr-29. The factors responsible for activating Tyr-29 remain unclear, although some structural changes around Ser-254′, Asp-96, and Glu-63, common to both complexes, suggest that those residues play a function. The role of Glu-289′ as the activator of Tyr-29, previously postulated for the closely related *Pseudomonas 7A* L-glutaminase-asparaginase, is not confirmed in this study, due to the lack of interactions between these residues in these complexes and in holoenzymes. The results reported here are consistent with previous reports that mutants of *Escherichia coli* L-asparaginase lacking Glu-289 remain catalytically active and prove the catalytic roles of both Thr-15 and Tyr-29, while still leaving open the question of the exact mechanism resulting in the unusual chemical properties of these residues. © 2001 Elsevier Science B.V. All rights reserved.

Keywords: Bacterial L-asparaginase; Enzymatic mechanism; X-ray crystallography; Suicide inhibitor

1. Introduction

L-Asparaginase (L-asparagine amidohydrolase, EC 3.5.1.1) is an enzyme whose primary function is to catalyze the conversion of L-asparagine to L-aspartic acid and ammonia. Other substrates of this enzyme include D-Asn, L- and D-Gln, and succinic acid monoamide [1,2]. The products of the hydrolysis were also shown to function as substrates at acidic pH [3,4]. In this case the reaction, delineated by isotope exchange, involves the replacement of carboxyl oxygens [5].

Two bacterial L-asparaginases, isolated from either *Escherichia coli* (EcA) or *Erwinia chrysanthemi* (ErA), have been used since the early 1970s in the treatment of acute childhood lymphoblastic leukemia [6,7]. The basis of their clinical activity is attributed to the reduction of L-asparagine circulating in blood. Since some neoplastic cells depend on extracellular supplies of this amino acid, they are selectively killed during L-asparagine deprivation [8].

To date, five L-asparaginases from different bacterial sources have been studied by means of X-ray

---

crystallography. Structures of the holoenzymes have been reported for *Acinetobacter glutaminasificans* (AGA) and *Wolinella succinogenes* (WsA) L-asparaginases [9,10]. In the reported structures of EcA and ErA, the active sites were sometimes occupied by the substrate, L- or D-aspartic acid, L-glutamic acid or succinic acid [3,4,11]. Additionally, structures have been published for ErA and *Pseudomonas 7A* L-asparaginase (PGA) with SO_4^{2-} located in the active sites [4,12,13], as well as for covalent complexes of PGA with 6-diazo-5-oxy-L-norleucine (DON) and with 5-diazo-4-oxo-L-norvaline (DONV) [14]. Determination of the crystal structure of the T89V active site mutant of EcA [15] led to the description of an acyl-enzyme intermediate and to the identification of the catalytic nucleophile. Finally, some otherwise comparable structures of L-asparaginases were solved in multiple crystal forms [16].

The numerous structural studies of L-asparaginases mentioned above provided a detailed description of the common structural features of these enzymes. All bacterial L-asparaginases are active as homo-tetramers with 222 symmetry and their molecular mass is in the range of 140–150 kDa. A monomer consists of about 330 amino acid residues that form 14 β strands and eight α helices, arranged into two easily identifiable domains, the larger N-terminal domain and the smaller C-terminal domain, connected by a linker consisting of ∼20 residues (Fig. 1). Each of the four identical and non-cooperative active sites of L-asparaginase is located between the N- and C-terminal domains of two adjacent monomers (Fig. 1) [3]. Structurally rigid regions of the active sites are formed by a topological switch point [17] between the first and the third parallel β strands of the N-terminal domain, and by the residues extending from the loops of the C-terminal domain of the adjacent monomer [3,4]. The flexible part of the active site consists of several residues (14–33 in ErA), referred to as the active site flexible loop, and covers the binding pocket upon substrate binding to the enzyme [12,18]. The nucleophile initiating the enzymatic reaction, Thr-15$_{ErA}$, is also located in the flexible loop region [15].

In addition to structural studies, numerous kinetic experiments have been conducted for L-asparaginases in order to elucidate the catalytic mechanism and the substrate specificity of these enzymes. The enzymatic reaction catalyzed by these enzymes proceeds according to a two-step ping-pong mechanism similar to the mechanism of serine proteases [5], except that the attacking nucleophile is a threonine. Thr-12$_{EcA}$ (corresponding to Thr-15$_{ErA}$) has been identified as the primary nucleophile [15]. The first tetrahedral acyl-enzyme intermediate is formed after a nucleophilic attack by this threonine on the carboxylic carbon of the substrate. The latter undergoes a nucleophilic attack by the water (or OH^-) molecule, and the second tetrahedral intermediate converts finally into the products.

One of the unexplained questions regarding the details of such a mechanism is how the usually weak nucleophilicity of a threonine is raised to a level sufficient to initiate the reaction. It is known from kinetic studies of mutated EcA [19] that a tyrosine residue structurally adjacent to the nucleophilic threonine (Tyr-29$_{ErA}$) is critical for the activity. Recently, Ortlund et al. [14] reported crystal structures of covalent complexes between PGA and two suicide inhibitors, DON and DONV, showing direct involvement of the active site tyrosine in the catalytic process by subtracting a proton from the nucleophile's hydroxyl group. The currently available evidence does not provide, however, satisfactory understanding of the initial events of the catalytic reaction, since tyrosine is not by itself a strong base, especially at pH higher than 8 or 9, i.e., under conditions at which L-asparaginases are still potent enzymes [20–23]. Ortlund et al. [14] assigned the role of the base to the charged glutamate residue residing on an adjacent subunit (Glu-294′ in PGA, -289′ in ErA, and -283′ in EcA), and declared the motif Thr-Tyr-Glu to be the catalytic triad in bacterial L-asparaginases.

In this report we describe X-ray structures of ErA complexed with two stereoisomers of a suicide inhibitor, 6-diazo-5-oxy-L-norleucine (L-DON) and 6-diazo-5-oxy-D-norleucine (D-DON). These structures will be referred to as ErAL for the complex with L-DON and ErAD for the complex with D-DON. We will show that the proposed catalytic triad [14] does not appear to exist in ErA. We will also discuss this result in view of the published enzymatic data for EcA that indicate that the proposed triad is unlikely to be present in that enzyme as well.
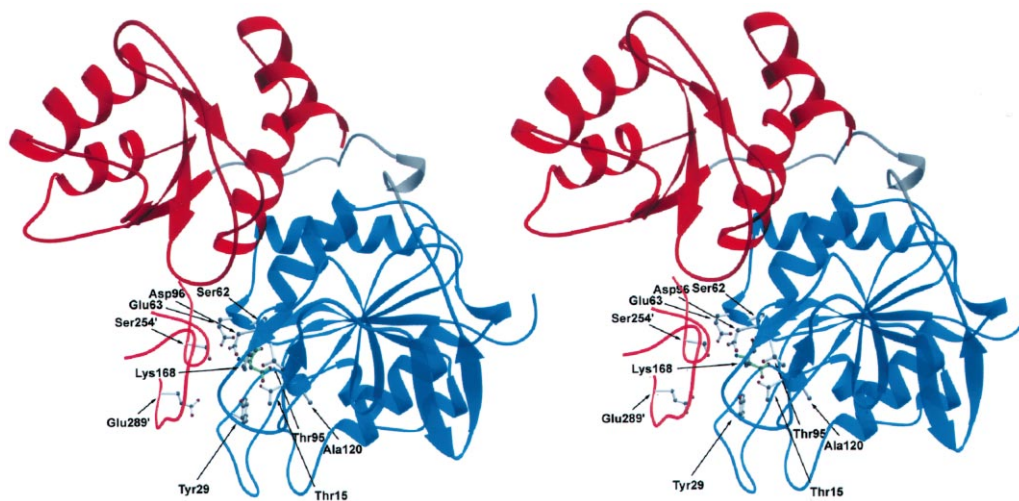
Fig. 1. Schematic representation of the ErA monomer. The N-terminal domain is shown in blue, C-terminal domain in red, and the linker region in gray. The active site residues are shown in ball-and-stick representation with labels. A fragment of the second monomer that contributes to the active site is shown in light red. Residues from the second monomer are marked with primes. The figure was prepared using the program RIBBONS [37], followed by rendering with the program POV-Ray (http://www.povray.org).
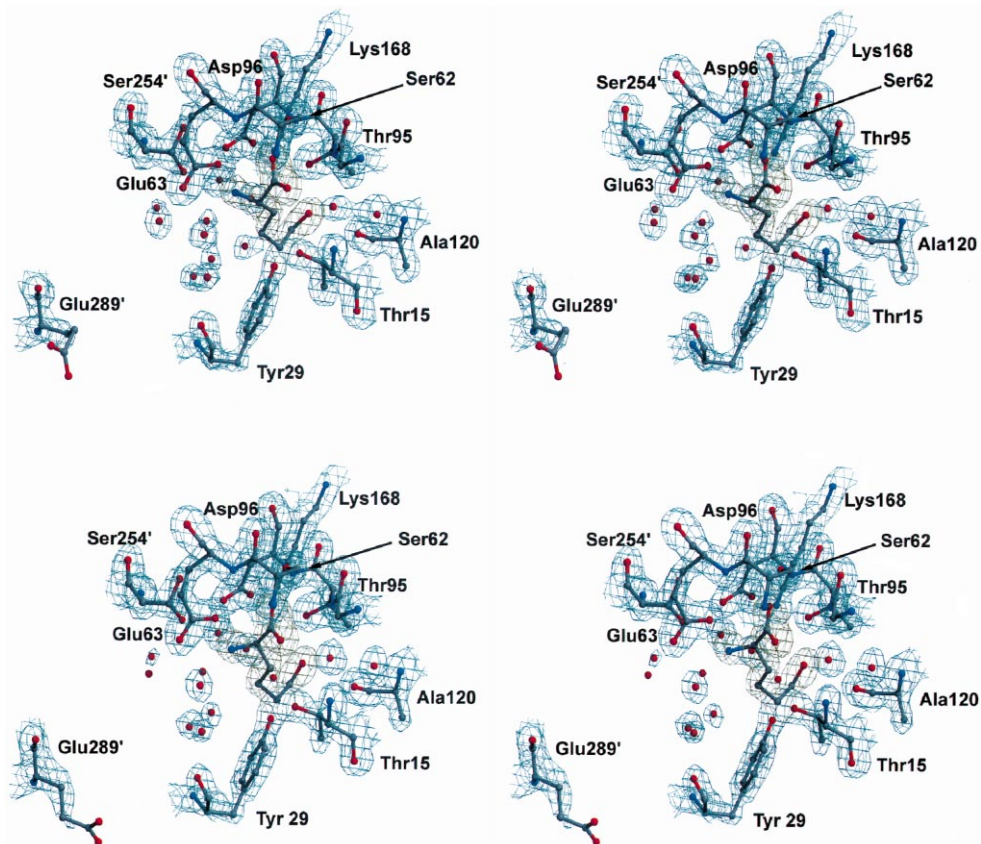
Fig. 2. Stereo representation of the final $2F_o$–F_c electron density maps for the active sites of the complexes between ErA and L-DON (top) and D-DON (bottom). Both maps are contoured at 1.2F, with the maps corresponding to the enzyme residues colored in blue whereas those corresponding to the ligand molecules shown in khaki. Unlabeled spheres, shown in red, represent water molecules. These active sites are representative for each complex in terms of the structure as well as the quality of the electron density maps. This and all the following figures were prepared using the program Bobscript [38], followed by rendering with the program POV-Ray (http://www.povray.org).

Table 1
Data processing and refinement statistics

	Complex of ErA with L-DON	Complex of ErA with D-DON
Temperature	100 K	100 K
X-ray source (wavelength, Å)	Rotating anode (1.5418)	Rotating anode (1.5418)
Space group	C2	C2
Unit cell parameters	$a = 106.07$, $b = 90.36$, $c = 127.401$, $\beta = 91.35$	$a = 106.15$, $b = 90.39$, $c = 127.37$, $\beta = 91.38$
Resolution limits (Å)[a]	20.0–1.65, (1.69–1.95)	20.0–1.70, (1.74–1.70)
R_{symm}^b	0.100 (0.430)	0.083 (0.442)
Total no. of observations	323 188	355 082
No. of independent observations	135 872	122 183
Completeness (%)[b]	93.8 (91.1)	92.0 (80.5)
Average $I/\sigma_I^{b,c}$	9.9 (2.2)	11.5 (2.2)
Refinement statistics		
No. of reflections ($I > 1*\sigma_F$)		
working set	117 007	113 524
test set	2410	1368
Resolution range (Å)	20.0–1.70	20.0–1.70
R-factor (Free-R)	0.183 (0.210)	0.186 (0.211)
Total no. of non-hydrogen atoms		
with occupancy 1.0	10 619	10 655
with occupancy < 1.0	838	560
No. of water molecules	1085	1164
Average B-factor (Å²)		
all non-hydrogen atoms	15.12	19.17
protein atoms	13.94	18.38
water molecules	22.00	27.11
Root-mean-square deviations from ideality		
bonds	0.006	0.006
valence angles	1.40	1.38
dihedrals	23.4	23.6
impropers	0.769	0.757

[a] Numbers in parentheses describe the high-resolution limits.
[b] Values shown in parentheses correspond to the high-resolution shell.
[c] I and σ_I describe the intensity and the standard deviation of intensity of reflection.

2. Materials and methods

2.1. Crystallization of ErA and preparation of the complexes

The sample of ErA used for all crystallization studies described here was a generous gift from the Intramural Research Support Program, SAIC–Frederick, where it was isolated and purified. The sample was subsequently used by us without any further purification. Crystals used for the diffraction experiments were grown using the protocol described previously by Miller et al. [4]. Monoclinic crystals appeared after 2–3 days and grew to their final size (deformed prisms, $0.5 \times 0.5 \times 0.5$ mm) within a few weeks. The inhibitors were bound to the active sites of the enzyme after adding small amounts of solid L-DON or D-DON to the droplets with freshly grown protein crystals, as described by Ortlund et al. [14]. Bubble formation in the droplets could be observed within 1 h due to the release of gaseous nitrogen during the reaction between the protein and inhibitors. The reaction was allowed to proceed for 24–36 h. Before collection of the X-ray data, crystals were transferred briefly to a solution equivalent in contents to the original mother liquor but with added glycerol (20% v/v) as a cryoprotecting agent.

2.2. Data collection and processing, structure solution, and refinement

X-ray data for both complexes of ErA were collected from a single crystal each at liquid nitrogen temperature using a conventional radiation source (wavelength 1.54178 Å). Data were recorded with a MAR Research 345 image plate detector mounted on a Rigaku RU-200 rotating-anode generator, operated at 50 kV and 100 mA. Both data sets were processed and scaled using the HKL2000 suite of programs [24]. The statistics for both data sets are shown in Table 1.

The initial model for the refinement was derived from the published structure of the complex between ErA and D-Asp [11]. Structure refinement as well as calculation of electron density maps were performed with the program CNS-XPLOR [25], whereas visual inspection and manual rebuilding utilized the program O [26]. For both complexes, 1.2–2.2% of randomly selected experimental data were excluded from structural refinement and used for cross-validation purposes [27]. All water molecules and the D-aspartate bound in the active site of the search structure were removed. A rigid-body protocol was applied as the first step of refinement at the resolution of 20–2.3 Å to compensate for the differences in the unit cell parameters. Subsequently, the individual positions and B-factors of all nonhydrogen atoms were refined and the resolution was extended to the limits of experimental data.

The initial electron density maps revealed the presence of inhibitor molecules bound in the active sites of the enzyme. After several rounds of refinement and model improvement, all atoms in either L-DON or D-DON molecules could be seen in the $2F_o–F_c$ and $F_o–F_c$ electron density maps. It was also very clear that inhibitor molecules were covalently bound to the hydroxyl oxygens of both Thr-15 and Tyr-29 (Fig. 2). These observations allowed us to continue refinement with L- or D-DON molecules modeled in all four active sites of ErA. The topology and parameters libraries for the L-DON and D-DON were generated based on those used by CNS-XPLOR for L-Glu [28], as well as used by us previously in refinement of complexes between ErA and D-Asp and succinic acid [11].

The presence of covalent bonds between the inhibitors and the protein was not enforced, but the repulsive interactions between covalently bound atoms were omitted during energy minimization. Therefore, the location of inhibitor molecules relative to Thr-15 and Tyr-29 relied only on the experimental data, minimizing any refinement-induced bias. During the course of refinement, inspection of electron density maps led to the location of the water molecules and to the assignment of multiple conformations of protein residues, as well as to the introduction of necessary corrections to the models. Several clusters of peaks found in the $F_o–F_c$ electron density map could not be attributed to water molecules. Four of such clusters found in EraL and three found in ErAD agreed in their shape and dimensions to glycerol molecules, present in solution as cryoprotectant, and they were included in the models. The intriguing torus-like electron density located near the NZ atom of Lys-243 in one of the ErA monomers, and perpendicular to the extended side-chain of this residue, was observed by us previously in all other structures obtained under cryogenic conditions. We modeled this density as corresponding to low molecular mass polyethylene glycol, also present in the crystallization solution. A decrease in free-R value, very good agreement with the electron density peaks, as well as chemically correct interatomic contacts suggested that this guess was most likely correct. The complete models were subsequently refined to convergence, and the assessment of the geometrical and stereochemical quality was performed with programs PROCHECK [29] and WHATIF [30]. The final statistics from the structural refinement and the basic characteristics of the models are shown in Table 1.

3. Results

3.1. General structural features of the models

The overall fold of the enzyme is virtually identical to those previously published for ErA [4,11] and other bacterial L-asparaginases [3,9,10,12]. Therefore, we will limit our description to the features that are specific to the structures reported here. The structures of both complexes were refined to a relatively high resolution of 1.7 Å, and in both cases data were acquired at liquid nitrogen temperature. These sim-

ilarities resulted in high consistency between the structures and minimized possible variations of the experimental errors. The first three N-terminal amino acids could not be modeled in any of the four independent monomers in each structure. By contrast, the C-terminal residues are all well ordered, resulting in models for residues 4 through 327 in all peptide chains. This feature is common to all bacterial L-asparaginases studied so far by means of X-ray crystallography. A number of residues could be modeled in two conformations. Such residues in ErAL are Leu-10, Val-43, Ser-74, Glu-100, Ser-128, Leu-136, Val-208, Ser-216, Ser-254, Glu-288, Leu-293, Leu-298, and Leu-309 in chain A; Leu-10, Leu-34, Lys-48, Met-60, Leu-71, Ile-127, Ser-172, Arg-198, Arg-206, Ser-216, Lys-243, Ser-254, Glu-288, Glu-289, and Met-308 in chain B; Asn-51, Val-89, Arg-140, Ile-199, Arg-206, Thr-215, Ser-254, Val-255, Ile-260, Lys-269, and Arg-313 in chain C; and Thr-24, Asp-37, Val-46, Arg-76, Val-89, Ser-101, Asp-112, Leu-136, Arg-140, Ser-162, Ser-172, Ser-254, Ile-260, and Met-308 in chain D. Residues with dual conformations observed in the structure of ErAD are Val-8, Val-43, Met-65, Lys-72, Leu-136, Ile-160, Val-208, Ser-254, and Thr-326 in chain A; Leu-10, Leu-34, Ser-74, Ile-199, Glu-231, Ser-254, Glu-289, and Ser-297 in chain B; Leu-4, Leu-10, Asn-51, Arg-83, Leu-202, and Ser-254 in chain C; and Lys-53, Ser-216, Ser-254, and Ile-283 in chain D. Some of the disorder can be explained by crystal contacts, for example Val-43 or Val-208 accommodating double conformation of their side chains only in the chain A of both complexes. For a few residues, such as Leu-10, Leu-136, and Ser-216, discrete disorder was detected in most of the monomers, and seems to be the intrinsic property of their side chains. For many other residues listed above, disorder results from either lack of interactions due to their location on the surface of the protein or might be a simple artifact of experimental data. The side chain of Ser-254, however, is systematically disordered between two well-defined orientations in all protein chains. All alternate conformations were modeled with equal occupancy of 0.5. In case of Ser-254, one of the conformations is identical to that observed previously in other structures of ErA [4,11] as well as AGA [9] and PGA [12,13]. In this conformation, the hydroxyl group of the serine forms short hydrogen bonds with the side chain of Asp-96 of the intimate monomer and with a water molecule. In the second rotamer of the Ser-254 side chain, the hydroxyl group relocates away from both Asp-96 and the water molecule, and in turn forms a hydrogen bond with the main chain carbonyl of Met-250 from the same monomer. Based on the electron density maps, this new conformation found for Ser-254 appears to be dominating in all active sites of ErAL and ErAD. Because Ser-254 is located in the active site of ErA, we believe that its conformational change is associated with the particular protonation states of some active site residues, as a result of covalent binding of the inhibitor molecules.

Three glycerol molecules were modeled into corresponding areas of the electron density in both structures. They are located on the surface of the ErA tetramer, adjacent to the tripeptide stretches Arg-83–Asp-85, Gly-213–Thr-215, and Arg-313–Ser-315, respectively. Additionally, in ErAL we identified another glycerol molecule buried in the cavity located near the center of the tetrameric assembly. This cavity is surrounded by the equivalent fragments consisting of residues Arg-178 through Tyr-184 from the four protein chains. In each of the structures we modeled one pentaethylene glycol molecule [HO-$(CH_2CH_2O)_5$-H]. Strong, positive horseshoe-shaped F_o–F_c electron density peak, surrounding the tip of extended side-chain of Lys-243, was clearly observed already in the initial experimental maps. Our model of a molecule with the mass of 238 Da agrees well with the fact that 2% of polyethylene glycol (average molecular mass 400 Da) was present in the crystallization solution.

3.2. Conservation of water structure

The positions of water molecules were determined independently in ErAL and ErAD since the model used to initiate the refinement of both structures consisted of only protein chains. Positions of all solvent molecules were visually inspected for agreement with electron density peaks as well as chemical environment. We found 1085 water molecules on the structure of ErAL, and 1164 in that of ErAD. Using program WHATIF [30] we assigned water molecules in each complex to specific monomers. The number of water molecules associated with monomers A through D in ErAL was found to be 232, 210, 236,
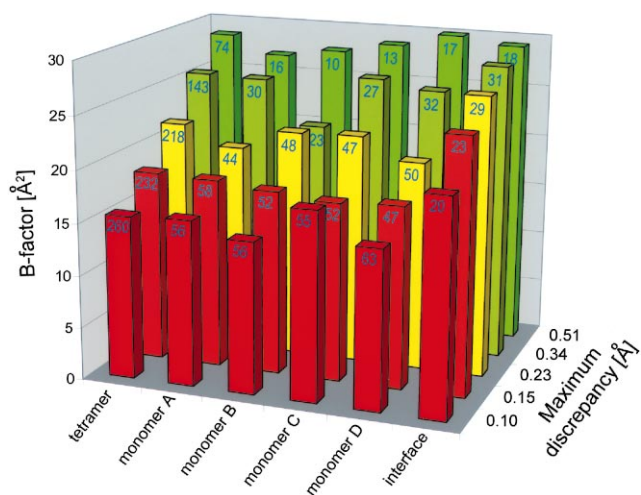
Fig. 3. A diagram representing conservation of the water structure in the complex of ErA with L-DON. The numbers at the top of each bar represent water molecules. The height of the bars is proportional to the B-factors averaged over the contributing water molecules. An equivalent diagram for the complex between ErA and D-DON would be very similar. For more details on the preparation of this diagram see text.

quently, we analyzed conservation of the solvent structure in both complexes. Both structures were superimposed on the basis of their Cα atoms using the program ALIGN [31]. Using the discrepancy of positions in the two complexes, water molecules were divided into six subsets (maximum discrepancies allowed for each subset were 0.1, 0.15, 0.23, 0.34, 0.51, and over 0.51 Å). The number of pairs of water molecules that deviated less than 0.51 Å was 927, representing 80–85% of all water molecules in both complexes. A more detailed analysis of the degree of solvent conservation is presented in Fig. 3, where several trends can be observed. Water molecules with more conserved positions are also characterized by lower B-factor values. When only the water molecules occupying positions conserved in both complexes within 0.1 Å are considered, their average B-factor values (15.55 Å^2 in ErAL, and 19.66 Å^2 in ErAD) are comparable to the average B-factors of protein atoms (see Table 1). Within a single range, solvent molecules located in the interfaces between protein monomers have higher B-factor values compared to the molecules clearly associated with specific monomers. This observation, however, does not hold when the higher deviations (more than 0.23 Å) are allowed. Within 10% range, comparable numbers of solvent molecules are associated with each monomer, and there are more conserved waters bound to any

and 236, respectively. In ErAD we assigned 240, 238, 240, and 240 water molecules, respectively, to the four monomers. The remaining 171 water molecules in ErAL and 206 in ErAD are located in the interfaces between monomers, and cannot be unambiguously associated with unique protein chains. Subse-
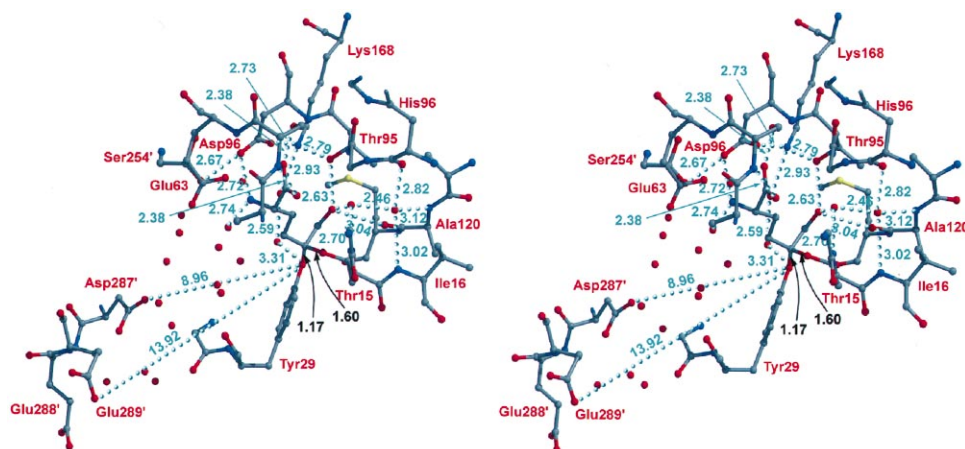
Fig. 4. Stereo representation of the active site of the complex between ErA and L-DON. Residues are identified by red labels, with primes denoting residues from the second monomer. The network of hydrogen bonds is indicated by sequences of blue dots and the corresponding distances (in Å) are marked. The two long distances between negatively charged side chains from the second monomer and the hydroxyl group of active site Tyr-29 are also shown. Two values, printed in black, correspond to the bond lengths between Cα of the L-DON, and the hydroxyl oxygen atoms of Thr-15 and Tyr-29. Although bond lengths are taken from a single monomer of the complex, their values are representative for all active sites in ErAL and ErAD.

specific monomer than located in the interfaces. As above, this is not the case for solvent with deviations higher than 0.23 Å.

3.3. Structures of the active sites

Covalent binding of the inhibitor molecules to the ErA active sites significantly stabilized conformations of all residues compared to the holoenzyme [9,10,12] or even to the enzyme with noncovalently bound ligands [4,11]. Therefore, nearly all active site atoms are not only very well defined in the electron density (Fig. 2) but are also characterized by quite low B-factors. This is especially pronounced for the flexible loop region (residues 14 through 33) which is so disordered in unliganded bacterial L-asparaginases that its structure cannot be determined at all [10,12]. Within each complex, the structures of the active sites are very highly conserved. The root-mean-square deviation between corresponding Cα atoms of any pair of active sites is lower than 0.2 Å. This structural conservation is also found between both complexes. The only clear, yet very small, conformational difference results from different stereochemistry of L-DON and D-DON. Interestingly, this difference is manifested just by small relative discrepancies between the locations of α-NH_3^+ and adjacent Cα atoms in the stereoisomeric inhibitor molecules. Therefore, specific interactions between the inhibitor molecules and protein are the same in both complexes. Despite covalent binding of Thr-15 and Tyr-29 to the inhibitor molecule, the remainder of the active site assumes a conformation virtually identical to that previously determined for other complexes of ErA [4,11], with the single exception of the side chain of Ser-254. An observation that the B-factors of the atoms in the protein and in the inhibitor that are covalently bound are the same indicates full occupancy of the inhibitor, a result of the irreversible nature of the reaction. The extensive similarity of the active site structures of both complexes also extends to the associated water molecules. We could identify more than 10 water molecules occupying identical positions in all eight active sites (four in each complex). A majority of these water molecules are characterized by low-to-moderate B-factors. Electron density peaks are more diffused for only a single water molecule, suggesting that it may be more labile than the rest of the active site.

As seen in Fig. 4, solvent plays a very important role in the formation of a hydrogen-bonded network in the active site. As mentioned above, two active site residues, Thr-15 and Tyr-29, are covalently bound to the Cδ of inhibitor molecule. The presence of covalent bonding is manifested by very strong, continuous electron density between participating atoms. Furthermore, distances between the hydroxyl oxygen atoms of Thr-15 and Tyr-29, and the Cδ of inhibitor are very short, 1.2 and 1.6 Å, respectively. We would like to stress that these distances were not forced by any restraints utilized during the refinement, but resulted only from the experimental data. Formation of covalent bonds between the protein and inhibitor resulted in some movement of the active-site flexible loop (in particular residues Thr-15 and Tyr-29) towards the inhibitor molecule, as compared to their positions observed in complexes between ErA and other ligands [4,11]. In all active sites of both cova-

→

Fig. 5. Comparison of primary and tertiary structures of different bacterial L-asparaginases. (A) An alignment of amino acid sequences of L-asparaginases from five bacterial sources. Residues common to all enzymes are shown in red, those common to four enzymes are shown in magenta, and the lowercase letter indicates non-conserved amino acid. Positions at which sequence conservation is correlated with enzyme specificity are marked in gray-outlined yellow. These are residues that are different in highly specific L-asparaginases (WsA and EcA) than in L-glutaminase-asparaginases (AGA and PGA), or in ErA. Positions conserved among WsA, EcA, and ErA are shown in green, while in blue when conservation spans over ErA, PGA, and AGA. Residues marked in gray are chemically conserved in all five enzymes (i.e., all hydrophobic). Colored boxes mark the residues forming the active site pockets. In particular, the region of sequences indicated by a red box contains Glu-294$_{PGA}$, postulated to play the role of a catalytic base [14]. Red asterisks mark the active site residues (numbered for ErA), assumed to play some role in catalysis. Boundaries of the N- and C-terminal domains and the linker region are shown with arrows. (B) Stereo representation of the superimposed active sites from complexes between ErA (carbon atoms shown in gray) or PGA (green carbon atoms) and L-DON. Water molecules shown in darker red shade belong to the ErA complex. Several water molecules are present in ErA in the position occupied by Glu-294$_{PGA}$. The corresponding Glu-289$_{ErA}$ is very distant from the active site, although the remaining active site residues from both complexes align very well.

lent complexes we found the hydroxyl oxygen of Ser-254 in two alternate positions, suggesting that its interactions are possibly linked to the loss of protons on Thr-15 or Tyr-29, or both. We base this statement on the fact that this twofold disorder of Ser-254 side chain was not observed previously in any other complexes of ErA. Finally, yet very importantly, we did not observe any significant change in the conformations of residues around Glu-289 when compared to the previously determined structures of ErA. Despite
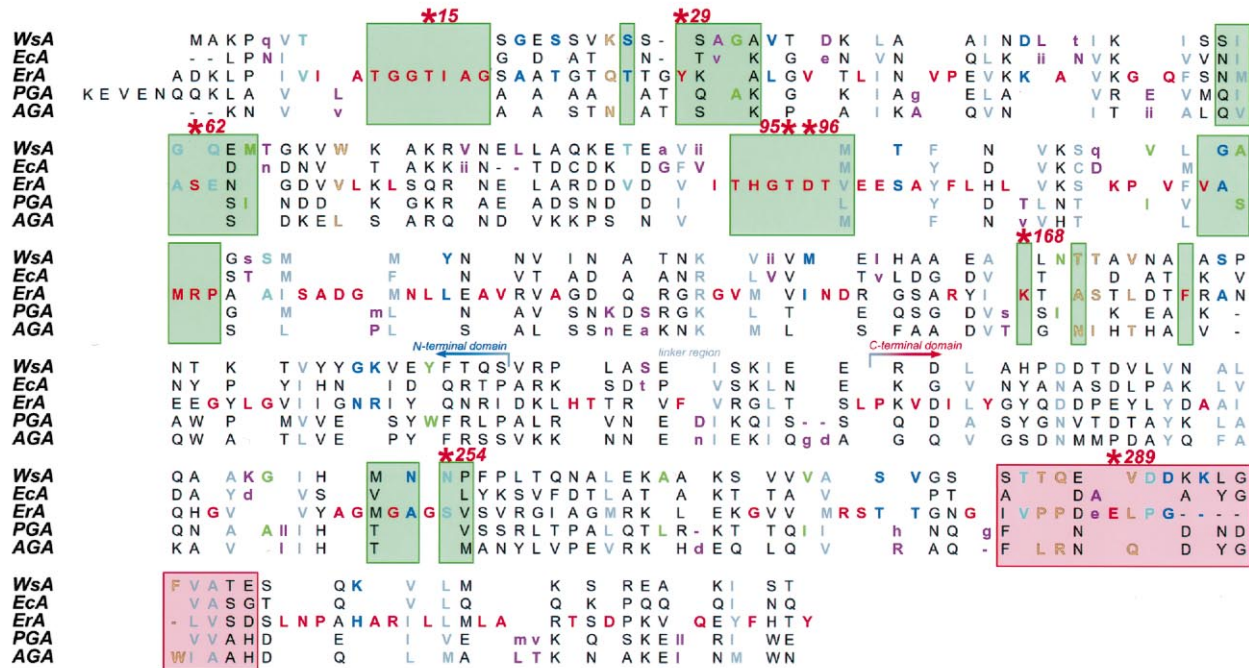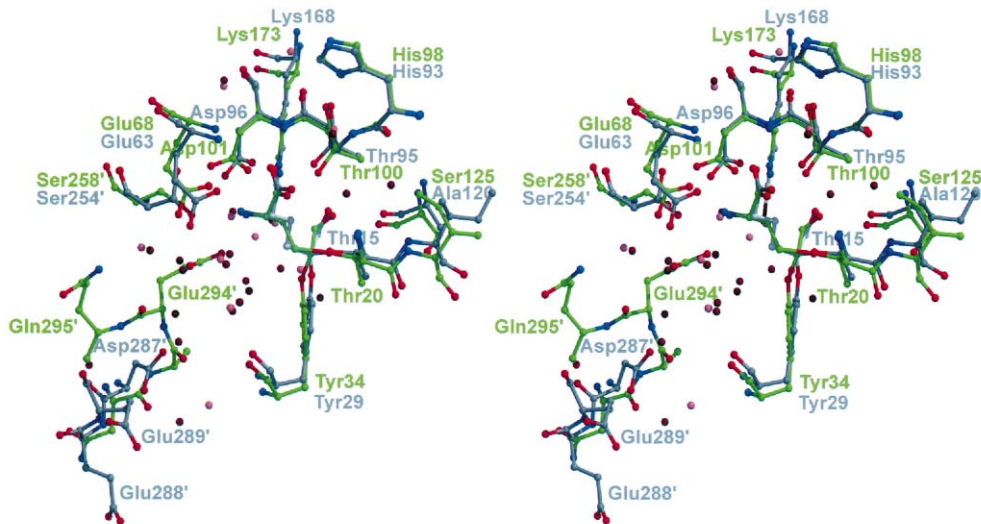
some moderate disorder of the side chain of Glu-289 previously reported for ErA [4,11], as well as for several other bacterial L-asparaginases [3,9,10], the distance between the closest atom of this residue and the hydroxyl group of Tyr-29 always exceeds 12 Å.

4. Discussion

The primary reason for this determination of the crystal structures of the complexes of ErA with suicide inhibitors was to validate or disprove the postulated role of Glu-289$_{ErA}$ in the catalytic triad Thr-Tyr-Glu [14]. We found three major problems with the proposed model of the nucleophilic attack initiating the enzymatic reaction in bacterial L-asparaginases. In the previously published structures of ErA, the closest atom of Glu-289 is consistently located more than 12 Å away from the hydroxyl group of the catalytic Tyr. Therefore, it seems very unlikely that Glu-289 activates a Tyr in the process of proton-abstraction from the nucleophilic threonine. In the scenario presented by Ortlund et al. [14], the hydroxyl oxygen of tyrosine has to be in direct contact with both the hydroxyl oxygen of the nucleophilic threonine as well as with the negatively-charged glutamate side chain. Such a conformation could only be possible in ErA after extreme conformational readjustments of the region of several residues including Glu-289. That, however, was never observed previously for this enzyme, even when various substrate/ligand molecules were bound in the active site, nor can it be modeled in a plausible manner. The conformational difference between ErA and PGA in this area is a result of the differences between the amino acid sequences of the proteins. Fig. 5A shows the sequence alignment of L-asparaginases from five bacterial sources. In the region of Glu-289, marked by a red box, the sequence of ErA is shortened by several residues compared to other L-asparaginases, leading to its unique structure. Such structural differences between ErA and PGA are shown in Fig. 5B.

The structures presented here show that the interaction between ErA and suicide inhibitors L-DON and D-DON does not affect the conformation of Glu-289. As in all other structures of ErA complexes, we found the side chain of Glu-289 to be relatively flexible, although this feature is not unique to ErA. However, none of the possible conformations of Glu-289 could explain its role as the catalytic base. The only remaining possibility is that the enzymatic reaction in ErA follows a different mechanism than in PGA and other bacterial L-asparaginases. This very unlikely possibility is closely related to our next argument against the role of glutamate residue as the catalytic base.

Comparison of amino acid sequences (Fig. 5A) and crystal structures of PGA [12,13] and EcA [3] shows that the regions containing Glu-289 are very similar in both proteins. Therefore, the details of the enzymatic reaction are very likely to be the same for PGA and EcA. Wehner [32] and Schleper [33] conducted extensive kinetic studies on different mutants of EcA. Their work included three mutants of Glu-283 (EcA equivalent of the putative catalytic base), Glu-283Gln, Glu-283Gly, and Glu-283Val. They showed that the activity of mutants was only moderately impaired compared to the wild-type enzyme. While the k_{cat} and K_m values for the wild-type EcA were reported as 54 s^{-1} and 75 μM, they changed to 32 s^{-1} (1500 μM), 9 s^{-1} (660 μM), and 15 s^{-1} (1300 μM), for Glu-283Gln, Glu-283Gly, and Glu-283Val, respectively. These results clearly indicate that replacement of glutamate by non-charged, non-basic residues did not render the enzyme inactive. Moreover, these results, as well as our observations reported previously [11], suggest that this glutamate residue is primarily important for ligand binding and for specificity of bacterial L-asparaginases. By contrast, in the case of serine or cysteine proteases, where the catalytic role of the base has been clearly established, mutations of such base resulted in practically complete loss of the enzymatic activity [34,35]. No kinetic data are currently available in the literature for the mutants of PGA or for other bacterial L-asparaginases to verify directly the postulated catalytic role of Glu-294$_{PGA}$ in these enzymes. However, the arguments presented above do not support its catalytic role as suggested for bacterial L-asparaginases [14].

The third argument against the presence of an unusual catalytic triad, Thr-Tyr-Glu, in L-asparaginases in less direct, nevertheless might still be worth mentioning. An analysis of pH-activity profiles for different bacterial L-asparaginases [20–23], including PGA

[22] shows that these enzymes are quite active even at pH as low as 4. The pK_a value of the side-chain carboxylate of a glutamic acid, although dependent on exact chemical environment, averages around 4.1 [36]. Taking into account that the putative active site glutamate is located in most L-asparaginases in the proximity to other negatively charged residues (Asp-287 and Glu-288 in ErA; see Figs. 3 and 5), one could anticipate that in a substantial fraction of the active sites it will be in its protonated state at pH $\sim$ 4–5. The lack of a major decrease in the activity of L-asparaginases at low pH values points against the catalytic role of glutamate as a base.

An additional aspect of the discussion needs to address the differences between diazo-carbonyl inhibitors, such as DON or DONV, and amides, the natural substrates of bacterial L-asparaginases. Because of their significant differences in the chemical reactivity, with diazo-carbonyl-derivatives being quite reactive and amides rather inert, the question arises whether the mechanisms of enzymatic reactions of bacterial L-asparaginases necessarily follows the same pathways in both cases. The specific binding of DON (DONV) to the active site of L-asparaginases, is determined by the α-amino and α-carboxyl groups of these inhibitors, as is the case for natural substrates. While bound, however, the side chain of an inhibitor carrying diazo-carbonyl group is exposed to various chemical pressures posed by the surrounding residues. Under such circumstances, the chemistry of the reaction between diazo-carbonyl arrangement and the enzyme can be substantially different from that of natural substrates. This would furthermore weaken the proposed mechanism of hydrolysis of natural substrates by bacterial L-asparaginases, as was directly elucidated from the results obtained for complexes with suicide inhibitors.

In summary, we present here high-resolution structures of covalent complexes between ErA and its suicide inhibitors. Except for the first three amino acids, the conformation of all residues in each complex was determined with high accuracy, with particular care being taken in defining the solvent structure as well as location of ligand molecules. Based on these results, we cannot confirm the role of Glu-289 as the general base during catalysis [14]. In our opinion, the factors responsible for the activation of the nucleophilic Thr-15 and the role played by Tyr-

29 in bacterial L-asparaginases should still be considered as unresolved.

References

[1] H.E. Wade, R. Elsworth, D. Herbert, J. Keppie, K. Sargeant, A new L-asparaginase with antitumour activity?, Lancet 2 (1968) 776–777.

[2] J.B. Howard, F.H. Carpenter, L-Asparaginase from *Erwinia carotovora*, J. Biol. Chem. 247 (1972) 1020–1030.

[3] A.L. Swain, M. Jaskólski, D. Housset, J.K.M. Rao, A. Wlodawer, Crystal structure of *Escherichia coli* L-asparaginase, an enzyme used in cancer therapy, Proc. Natl. Acad. Sci. USA 90 (1993) 1474–1478.

[4] M. Miller, J.K.M. Rao, A. Wlodawer, M.R. Gribskov, A left-handed crossover involved in amidohydrolase catalysis. Crystal structure of *Erwinia chrysanthemi* L-asparaginase with bound L-aspartate, FEBS Lett. 328 (1993) 275–279.

[5] K.H. Röhm, R.L. Van Etten, The ^{18}O isotope effect in ^{13}C nuclear magnetic resonance spectroscopy: mechanistic studies on asparaginase from *Escherichia coli*, Arch. Biochem. Biophys. 244 (1986) 128–136.

[6] J.M. Hill, J. Roberts, E. Loeb, A. Khan, A. MacLellan, R.W. Hill, L-Asparaginase therapy for leukemia and other malignant neoplasms. Remission in human leukemia, J. Am. Med. Assoc. 202 (1967) 882–888.

[7] M.P. Gallagher, R.D. Marshall, R. Wilson, Asparaginase as a drug for treatment of acute lymphoblastic leukaemia, Essays Biochem. 24 (1989) 1–40.

[8] E.E. Haley, G.A. Fisher, D.A. Welch, The requirement for L-asparagine of mouse leukemia cells L5178Y in culture, Cancer Res. 21 (1961) 532–536.

[9] J. Lubkowski, A. Wlodawer, D. Housset, I.T. Weber, H.L. Ammon, K.C. Murphy, A.L. Swain, Refined crystal structure of *Acinetobacter glutaminasificans* glutaminase-asparaginase, Acta Crystallogr. D 50 (1994) 826–832.

[10] J. Lubkowski, G.J. Palm, G.L. Gilliland, C. Derst, K.H. Röhm, A. Wlodawer, Crystal structure and amino acid sequence of *Wolinella succinogenes* L-asparaginase, Eur. J. Biochem. 241 (1996) 201–207.

[11] K. Aghaiypour, A. Wlodawer, J. Lubkowski, Structural basis for the activity and substrate specificity of *Erwinia chrysanthemi* L-asparaginase, Biochemistry 4 (2001) 5655–5664.

[12] J. Lubkowski, A. Wlodawer, H.L. Ammon, T.D. Copeland, A.L. Swain, Structural characterization of *Pseudomonas* 7Å glutaminase-asparaginase, Biochemistry 33 (1994) 10257–10265.

[13] C.G. Jakob, K. Lewinski, M.W. LaCount, J. Roberts, L. Lebioda, Ion binding induces closed conformation in *Pseudomonas* 7Å glutaminase-asparaginase (PGA): crystal structure of the PGA-SO$_4^{2-}$-NH^{4+} complex at 1.7 Å resolution, Biochemistry 36 (1997) 923–931.

[14] E. Ortlund, M.W. La Count, K. Lewinski, L. Lebioda, Reactions of Pseudomonas 7A glutaminase-asparaginase with

diazo analogues of glutamine and asparagine result in unexpected covalent inhibitions and suggests an unusual catalytic triad Thr-Tyr-Glu, Biochemistry 39 (2000) 1199–1204.

[15] G.J. Palm, J. Lubkowski, C. Derst, S. Schleper, K.H. Röhm, A. Wlodawer, A covalently bound catalytic intermediate in *Escherichia coli* asparaginase: crystal structure of a Thr-89-Val mutant, FEBS Lett. 390 (1996) 211–216.

[16] M. Jaskólski, M. Kozak, J. Lubkowski, G. Palm, A. Wlodawer, Crystal structures of two highly homologous bacterial L-asparaginases: a case of enantiomorphic space groups, Acta Crystallogr. D 57 (2001) 369–377.

[17] C. Branden, J. Tooze, Introduction to Protein Structure, Garland Publishing, New York, 1991.

[18] H.P. Aung, M. Bocola, S. Schleper, K.-H. Röhm, Dynamics of a mobile loop at the active site of *Escherichia coli* asparaginase., Biochim. Biophys. Acta 1481 (2000) 349–359.

[19] C. Derst, A. Wehner, V. Specht, K.H. Röhm, States and functions of tyrosine residues in *Escherichia coli* asparaginase II, Eur. J. Biochem. 224 (1994) 533–540.

[20] K.A. Cammack, D.I. Marlborough, D.S. Miller, Physical properties and subunit structure of L-asparaginase isolated from *Erwinia carotovora*, Biochem. J. 126 (1972) 361–379.

[21] M. Ehrman, H. Cedar, J.H. Schwartz, L-Asparaginase II of *Escherichia coli*, studies on the mechanism of action, J. Biol. Chem. 246 (1971) 88–94.

[22] J. Roberts, Purification and properties of a highly potent antitumor glutaminase-asparaginase from *Pseudomonas 7A*, J. Biol. Chem. 251 (1976) 2119–2123.

[23] J.A. Distasio, R.A. Niederman, D. Kafkewitz, D. Goodman, Purification and characterization of L-asparaginase with anti-lymphoma activity from *Vibrio succinogenes*, J. Biol. Chem. 251 (1976) 6929–6933.

[24] Z. Otwinowski, W. Minor, Processing of X-ray diffraction data collected in oscillation mode, Methods Enzymol. 276 (1997) 307–326.

[25] A.T. Brünger, P.D. Adams, G.M. Clore, W.L. DeLano, P. Gros, R.W. Grosse-Kunstleve, J.S. Jiang, J. Kuszewski, M. Nilges, N.S. Pannu, R.J. Read, L.M. Rice, T. Simonson, G.L. Warren, Crystallography and NMR system: a new software suite for macromolecular structure determination, Acta Crystallogr. D 54 (1998) 905–921.

[26] T.A. Jones, M. Kieldgaard, Electron-density map interpretation, Methods Enzymol. 277 (1997) 173–208.

[27] A.T. Brünger, The free R value: a novel statistical quantity for assessing the accuracy of crystal structures, Nature 355 (1992) 472–474.

[28] R. Engh, R. Huber, Accurate bond and angle parameters for X-ray protein-structure refinement, Acta Crystallogr. A 47 (1991) 392–400.

[29] R.A. Laskowski, M.W. MacArthur, D.S. Moss, J.M. Thornton, PROCHECK: program to check the stereochemical quality of protein structures, J. Appl. Crystallogr. 26 (1993) 283–291.

[30] G. Vriend, WHAT IF: A molecular modelling and drug design program, J. Mol. Graph. 8 (1990) 52–56.

[31] G.E. Cohen, ALIGN: a program to superimpose protein coordinates, accounting for insertions and deletions, J. Appl. Crystallogr. 30 (1997) 1160–1161.

[32] A. Wehner, Ph.D. Thesis, Philipps-Universität, Marburg, Germany, 1993.

[33] S. Schleper, Ph.D. Thesis, Philipps-Universität, Marburg, Germany, 1999.

[34] S. Sprang, T. Standing, R.J. Fletterick, R.M. Stroud, J. Finer-Moore, N.H. Xuong, R. Hamlin, W.J. Rutter, C.S. Craik, The three-dimensional structure of Asn102 mutant of trypsin: role of Asp102 in serine protease catalysis, Science 237 (1987) 905–909.

[35] C.S. Craik, S. Roczniak, C. Largman, W.J. Rutter, The catalytic role of the active site aspartic acid in serine proteases, Science 237 (1987) 909–913.

[36] R.M.C. Dawson, D.C. Elliott, W.H. Elliot, K.M. Jones, Data for Biochemical Research, Clarendon Press, Oxford, 1986, pp. 1–63.

[37] M. Carson, RIBBONS 4.0, J. Appl. Crystallogr. 24 (1991) 958–961.

[38] R.M. Esnouf, Further additions to MolScript version 1.4, including reading and contouring of electron-density maps, Acta Crystallogr. D 55 (1999) 938–940.